How to cite: *Angew. Chem. Int. Ed.* **2024**, *63*, e202403633
doi.org/10.1002/anie.202403633

VIP **Ammonia Production** **Very Important Paper**

High-Performance Ammonia Electrosynthesis from Nitrate in a NaOH–KOH–H_2O Ternary Electrolyte

*Usman Bin Shahid, Yongjun Kwon, Yuan Yuan, Shuang Gu, and Minhua Shao**

Abstract: A glut of dinitrogen-derived ammonia (NH_3) over the past century has resulted in a heavily imbalanced nitrogen cycle and consequently, the large-scale accumulation of reactive nitrogen such as nitrates in our ecosystems has led to detrimental environmental issues. Electrocatalytic upcycling of waste nitrogen back into NH_3 holds promise in mitigating these environmental impacts and reducing reliance on the energy-intensive Haber–Bosch process. Herein, we report a high-performance electrolyzer using an ultrahigh alkalinity electrolyte, NaOH–KOH–H_2O, for low-cost NH_3 electrosynthesis. At 3,000 mA/cm^2, the device with a Fe–Cu–Ni ternary catalyst achieves an unprecedented faradaic efficiency (FE) of 92.5 ± 1.5 % under a low cell voltage of 3.83 V; whereas at 1,000 mA/cm^2, an FE of 96.5 ± 4.8 % under a cell voltage of only 2.40 V was achieved. Techno-economic analysis revealed that our device cuts the levelized cost of ammonia electrosynthesis by ~40 % ($30.68 for Fe–Cu–Ni vs. $48.53 for Ni foam per kmol-NH_3). The NaOH–KOH–H_2O electrolyte together with the Fe–Cu–Ni ternary catalyst can enable the high-throughput nitrate-to-ammonia applications for affordable and scalable real-world wastewater treatments.

Introduction

Nitrogen (N_2), the most abundant naturally occurring gas on Earth (~78 % of the atmosphere), serves little purpose unless "fixed" in the form of reactive nitrogen (Nr).[1] These 'fixed' Nr compounds play a fundamental role in sustaining and propagating all forms of life on Earth; from the tiniest bacteria to the 8 billion human population.[2] The extensive deployment of the Haber–Bosch process for Ammonia (NH_3) synthesis catapulted the anthropogenic Nr production tenfold to >150 teragrams a year,[3] which sustains about 50 % of the world population's need for nitrogen nutrition. However, the fixed and then released Nr have made the nitrogen cycle the most altered biogeochemical cycle, compared to any other element such as carbon.[1]

Natural denitrification processes that convert these Nr species back into N_2 remain, but they are not capable of matching the rate of Nr generation, causing continued accumulation of Nr in air, water, and soil. The rising Nr levels nevertheless have resulted in progressively detrimental impacts on our fragile ecosystems and health, including soil acidification, coastal eutrophication, air pollution, declining biodiversity, and groundwater contamination.[1] Among anthropogenic Nr species, waste nitrate (NO_3^-) is the most prevailing one, because of the highest oxidation state, at an estimated accumulation rate of 40 million metric tons of nitrogen per year. Some of the severe health hazards associated with NO_3^- include neural tube defects during pregnancy, infant methemoglobinemia aka 'blue baby syndrome', thyroidal diseases, and colorectal cancer.[4]

Recycling this massive waste NO_3-N back into NH_3, through the electrochemical reduction of nitrate (NO3RR), can greatly reduce the reliance on direct N_2 conversion to NH_3 via the Haber–Bosch process, helping close the nitrogen cycle and alleviating environmental stress. Notwithstanding the significant progress in the development of selective and active electrocatalysts for NO3RR,[5,6,15–21,7–14] the high-productivity and low-cost NO3RR with both high selectivity and high efficiency on a desired industrial scale of current density (>1,000 mA/cm^2) remains very limited.[8,21,22]

[*] U. B. Shahid, Y. Kwon, Y. Yuan, M. Shao
Department of Chemical and Biological Engineering, Hong Kong University of Science and Technology, Clear Water Bay, Kowloon, Hong Kong, P.R. China
E-mail: kemshao@ust.hk
S. Gu
Department of Mechanical Engineering, Wichita State University, Wichita, KS USA
M. Shao
Energy Institute, Hong Kong Branch of the Southern Marine Science and Engineering Guangdong Laboratory, and Chinese National Engineering Research Center for Control & Treatment of Heavy Metal Pollution, The Hong Kong University of Science and Technology, Clear Water Bay, Kowloon, Hong Kong, P.R. China
U. B. Shahid
Department of Chemistry and Chemical Engineering, Lahore University of Management Sciences, Lahore, Pakistan
M. Shao
Guangzhou Key Laboratory of Electrochemical Energy Storage Technologies, Fok Ying Tung Research Institute, The Hong Kong University of Science and Technology, Guangzhou,511458, China

Of the promising catalysts developed so far, most include derivatives of expensive noble metals and are often obtained through very complex synthesis techniques. Although inexpensive earth-abundant metals[7,10,18,20,21,23,24] have also emerged as promising candidates for NO3RR, their performance has been marred by moderate ammonia selectivity and/or large energy consumption for operation at industrially desirable current densities. The development of high-performance NO3RR catalysts with high ammonia selectivity, low energy consumption, and inexpensive materials cost is of paramount importance to achieve high ammonia productivity at industrially desirable current densities.

An unexpected yet promising avenue to attain high-productivity NO3RR is through a NaOH–KOH–H_2O ternary electrolyte with ultrahigh alkalinity. Very recently, we demonstrated the surprising capability of the ternary alkaline electrolyte to sustain high-current density NO3RR operations using a plain Ni wire mesh as cathode, leading to an ammonia productivity of 4,200 mA/cm^2 (ammonia-oriented partial current density) with a faradaic efficiency (FE) of 84.5 % under a cell voltage of 4.5 V. Clearly, lower cell voltage and higher ammonia selectivity are critically needed to promote the high-productivity NO3RR, therefore calling for the development of high-performance NO3RR catalysts tailored to take full advantage of the robust ternary alkaline electrolyte system.

Herein, we report a high-performance Cu–Fe–Ni ternary catalytic system for high-productivity NO3RR operation in the NaOH–KOH–H_2O ternary electrolyte. The ternary catalyst with equimolar combination achieved FEs of 96.5 ± 4.8 % at 2.40 V and 92.5 ± 1.5 % at 3.83 V at 1,000 and 3,000 mA/cm^2, respectively at 100 °C. The Cu–Fe–Ni ternary catalyst significantly outperforms any pristine metals (Cu, Fe, and Ni) under the same testing conditions, due to synergistic enhancement. The presence of Fe in the catalyst, more specifically the α-Fe_2O_3 phase, was observed to play a crucial role in granting the high ammonia selectivity and low energy consumption.

Results & Discussion

Pursuit of a High-Performance and Low-Cost Catalyst: Fe–Cu–Ni Ternary System

Various inexpensive earth-abundant metals and their derivatives have emerged as the forerunners for NO3RR albeit in simple aqueous systems, including Ni-based electrodes[9,25] with operation durability, Cu-based catalysts[6,20,26] with high ammonia efficiencies, and Fe-based ones[7,18,27] with high ammonia productivity. However, the applicability of those pristine/pure metallic catalysts in NaOH–KOH–H_2O ternary electrolytes is compromised due to the ultrahigh alkalinity environments.

Known for its excellent corrosion resistance in alkaline solutions,[28] pure Ni has been the intuitive choice of cathode in ultrahigh alkalinity systems. In addition, Ni has been reported to be increasingly selective for NH_3 at more negative overpotentials in highly alkaline systems.[29] Cu is also well-known for its remarkable propensity for reducing NO_3^- to NH_3 with high ammonia selectivity (> 90 %).[9] More interestingly, Cu–Ni alloys with proper compositional tuning tend to outperform their pure counterparts, at least in ambient aqueous electrolytes.[9] However, Ni, Cu, and Cu–Ni alloy (Monel 400) as electrocatalysts at high current densities ≥ 1,000 mA/cm^2 showed moderate NO3RR performance (65 %–82 % as the highest NH_3 FE) in NaOH–KOH–H_2O electrolyte (see Figure 1a–c).

Similarly, Fe has also been extensively reported for its modest ammonia faradaic efficiency (ca. 75 %) in alkaline systems.[7,30] In addition, its chemical stability is of concern under ultrahigh alkalinity.[28] Stainless steel (such as SS304) was considered a corrosion-resistant substitute for pure Fe, its performance was comparable with Cu Foil at 1,000 mA/cm^2, however, the ammonia efficiency plunged sharply (< 35 % NH_3 FE) at higher current densities (Figure 1a–c).

Considering Wu et al.'s[7] Fe single atom catalyst's high ammonia selectivity and productivity for NH_3 in simple aqueous electrolytes, we conjectured that the inclusion of Fe atoms into the Cu–Ni system may yield a synergistic effect—boosting the NO3RR performance in the NaOH–KOH–H_2O ternary electrolyte while leveraging the material's resilience of Cu–Ni binary system in the ultrahigh alkalinity. The inclusion of multiple redox-active metal ions at the catalytically active sites also helps buffer the multi-electron transfer process essential for NO3RR thus increasing overall performance.[31] In short, the Fe–Cu–Ni ternary catalytic system may offer unprecedented performance at industrially desirable current densities for low-cost and high-productivity NO3RR operation.

Synthesis and Characterization of Fe_xCu_y@Ni Ternary System

The traditional physical mixing approach can be used to synthesize the Fe–Cu–Ni ternary alloys, however, the synthesized ternary alloys obtained through such an approach often have large crystal sizes, and therefore a very limited electrochemically accessible surface area.[32] Alternatively, electrodeposition can overcome the drawback of the physical mixing approach to achieve atomic synergy among the three metal elements, resulting in improved NO3RR.[33] Modifying Zhang et al.'s[31] electrodeposition approach to synthesize the ternary alloys (core–shell structured Fe–Cu–Ni electrodes), we prepared a ternary alloy electrode intentionally free of the core–shell features. The electrochemical dealloying process used by Zhang et al.[31] to obtain the core–shell features relied upon preferential discharge of the Cu metal due to its higher chemical activity relative to Ni and Fe which left behind a metal oxide layer on the surface. Such an oxidized surface structure is not desirable considering the poor electrical conductivity of most metal oxides, therefore, was intentionally avoided. Our Fe–Cu–Ni ternary electrode (denoted as Fe_xCu_y@Ni, hereinafter, Table 1) was fabricated via chronopotentiometric electrodeposition of the three elements from an equimolar electrolyte bath onto a Ni foil substrate (detailed method described in electronic Supporting Information (ESI†)). The

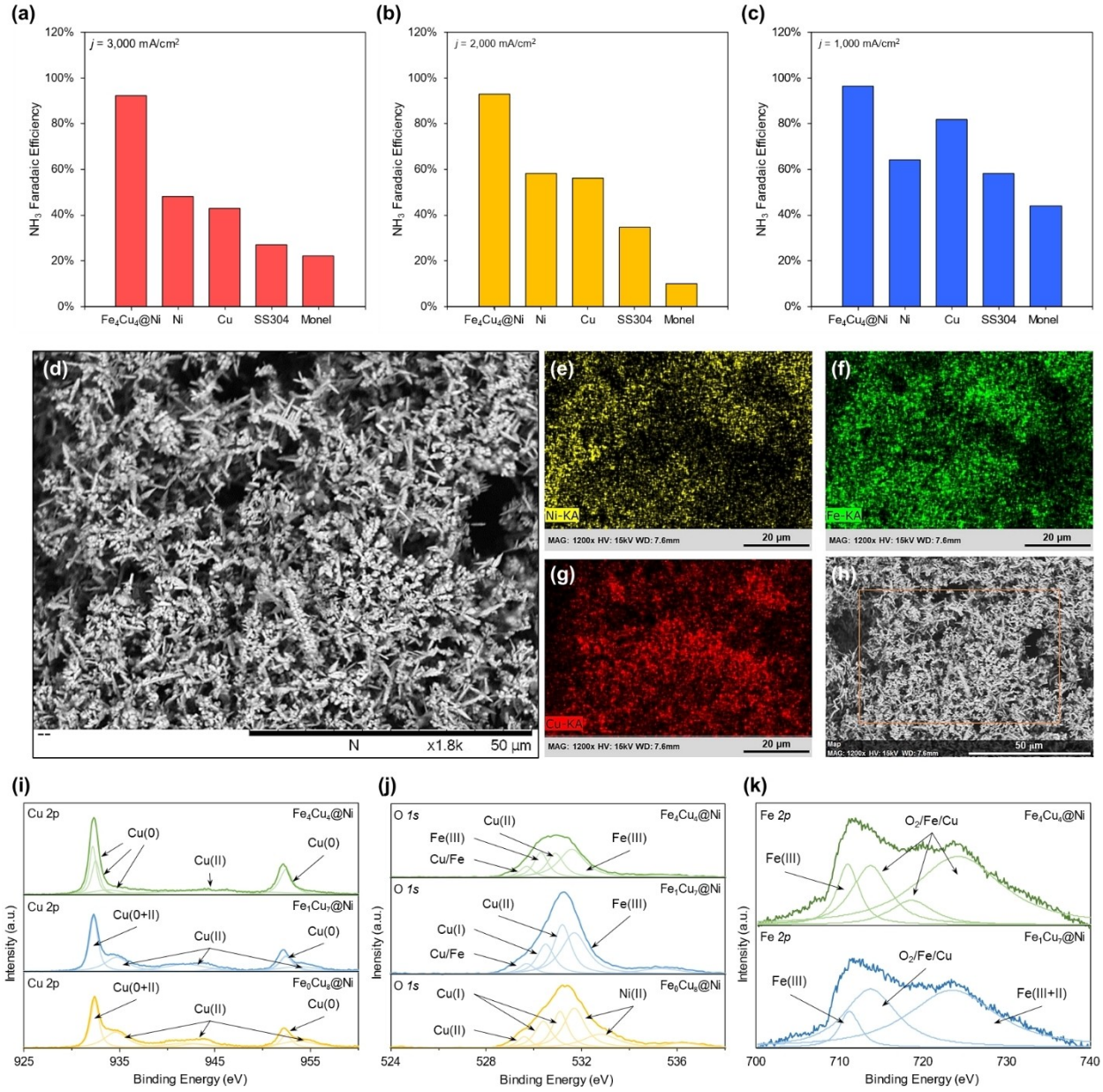

Figure 1. NO3RR performance and materials characterization of the Fe_4Cu_4@Ni catalyst. **(a)** NO3RR performance comparison at 3,000 mA/cm^2 of current density between the Fe_4Cu_4@Ni and four chosen common electrode materials. **(b)** and **(c)** NO3RR performance comparison at 2,000 mA/cm^2 and 1,000 mA/cm^2, respectively. **(d)** Scanning electron microscope (SEM) images of the as-prepared Fe_4Cu_4@Ni catalyst. Energy-dispersive X-ray spectroscopy (EDXS) elemental maps for **(e)** Ni, **(f)** Fe, and **(g)** Cu, **(h)** SEM of section probed for EDXS. A comparison of XPS profiles of **(i)** Cu *2p*, **(j)** O *1s*, and **(k)** Fe *2p* for Fe_0Cu_8@Ni, Fe_1Cu_8@Ni, and Fe_4Cu_4@Ni electrocatalysts.

atomic compositions of Fe:Cu:Ni in the deposited alloy at each electrode were then quantified through ICP-MS (Table S6–S7, ESI†) and the results correlated well with the electrolyte bath concentrations used for electrodeposition.

A uniformly dense distribution of dendritic structures with distinct tip-splitting and hierarchical features characterized the surface of the as-prepared catalyst when observed under the SEM (Figure 1d). Further, an elemental map for the SEM images was generated using an energy-dispersive x-ray spectroscopy (EDXS) technique which revealed a uniform distribution of three key elements: Ni, Fe, and Cu (Figure 1e–g). XPS analysis also confirmed the presence of the same three elements on the surface while deconvoluting the high-resolution spectrum for each, Cu *2p*, Cu *LMM*, Fe *2p*, and Ni *2p* signals suggested a mixture of pure and their corresponding oxide phases (Figure S5, ESI†). Moreover, an XPS depth profile revealed similar Fe–Cu–Ni atomic ratios as that at the surface indicating the successful co-deposition throughout the deposited layer (Table S11, ESI†). Rietveld refinement of the XRD scan of the Fe–Cu–Ni catalyst also confirmed the presence of four

Table 1: List of catalysts synthesized in this study with their recipes of precursors.

Catalyst Name	Cu : Fe Ratio	The Concentration of Metal Precursors in Electrolyte (mM)		
		$Fe(NO_3)_2 \cdot 9H_2O$	$CuSO_4 \cdot 5H_2O$	$NiCl_2 \cdot 6H_2O$
Cu_{10}	10 : 0	0	60	0
Fe_0Cu_8@Ni	8 : 0	0	40	20
Fe_1Cu_7@Ni	7 : 1	5	35	20
Fe_2Cu_6@Ni	6 : 2	10	30	20
Fe_3Cu_5@Ni	5 : 3	15	25	20
Fe_4Cu_4@Ni	4 : 4	20	20	20
Fe_5Cu_3@Ni	3 : 5	25	15	20
Fe_6Cu_2@Ni	2 : 6	30	10	20
Fe_7Cu_1@Ni	1 : 7	35	5	20

distinct crystalline phases: pure Cu, pure Ni, α-Fe_2O_3, and γ-Fe_2O_3 (Figure 3c).

High-Performance NO3RR of Fe_4Cu_4@Ni Ternary Catalyst

Voltametric studies of the Fe_4Cu_4@Ni alongside major control samples revealed the least negative onset potential for NO3RR in the NaOH–KOH–H_2O ternary electrolyte with 40 wt % of H_2O at 100 °C: −0.18 V on Fe_4Cu_4@Ni vs. −0.45 V on Cu foil and −1.02 V on Ni foil, against an Ag wire pseudo-reference electrode (Figure 2a). When compared with voltametric curve without NO_3^-, the change in the onset potential is also the largest on Fe_4Cu_4@Ni: 0.70 V cf. 0.38 V on Cu foil and 0.10 V on Ni foil. Both the least onset potential with NO_3^- and the largest change in onset potential (with vs. without NO_3^-) imply a very high NO3RR activity on Fe_4Cu_4@Ni.

The NO3RR performance was evaluated by means of a chronopotentiometry study. At 250 mA/cm^2 of constant current operation, around 100 % of NH_3 FE (i.e., FE towards NH_3, hereinafter) was observed on the Fe_4Cu_4@Ni ternary catalyst. The NH_3 FE slightly decreased to 96.5 %, 92.8 %, and 92.5 % at a current density of 1,000, 2,000, and 3,000 mA/cm^2, respectively, demonstrating the robust catalytic performance (Figure 2b). Among the three current densities tested here, Fe_4Cu_4@Ni is much more selective than all catalytic materials we tested including Ni, Cu, SS304, and Monel (a Cu–Ni alloy). Specifically at 3,000 mA/cm^2, the NH_3 FE of Fe_4Cu_4@Ni roughly doubles that of Ni (47 %) or Cu (43 %), triples that of SS304 (28 %), and quadruples that of Monel (23 %) (Figure 1). To the best of our knowledge, all those NH_3 FE values are the highest at the corresponding current densities in the NO3RR field.

The origin of produced NH_3 was confirmed to be from the catalytic reduction of NO_3^- in the electrolyte through a series of control experiments (Figure S7, ESI†). This catalytic reduction consisted of two components: a very minor spontaneous NO3RR and the dominating electrocatalytic NO3RR. The spontaneous NO3RR is the generation of ammonia from the introduction of the electrode without applying any current. Pure Fe,[34] pure Cu,[34,35] and Fe oxides,[36] all have been reported as chemically active for the spontaneous reduction of NO_3^- to NH_3. Nevertheless, the observed spontaneous NO3RR accounted for only 0.63 % of the total produced ammonia when operated at 1,000 mA/cm^2, and this component became increasingly insignificant when considering higher current densities. In all cases tested, the electrocatalytic NO3RR dominates the NH_3 formation.

Probing the reaction kinetics behind the electrochemical NO3RR, a reaction-order plot ($\log(i_{NH_3})$ vs. $\log(C_{NO_3})$, (Figure 2c) based on a variety of NO_3^- concentrations as the reactant feed showed that NO3RR follows a reaction order close to unity for experiments conducted at 1,000 mA/cm^2. Similar observations were also made for experiments carried out at 2,000 mA/cm^2 (Figure S9, ESI†).

To demonstrate the industrial practicality of the Fe_4Cu_4@Ni electrode, we conducted a chronopotentiometric stability test in a membrane-free alkaline electrolyzer (MFAEL). The Fe_4Cu_4@Ni electrode was operated at 1,000 mA/cm^2 for 24 hours with an initial NO_3^- concentration of 300 mM, with the electrolyte being replenished with NO_3^- at regular intervals of 4 hours. The overall potential remained stable throughout the test, leading to a 24-hour average ammonia efficiency of 102 % ± 5.9 % (Figure 2e). To further demonstrate the advantage of the NaOH–KOH–H_2O electrolyte over ambient electrolytes we recorded the performance of the same electrocatalyst at different temperatures in a 1 M KOH electrolyte containing 0.5 M $NaNO_3$. We observed that the full cell voltages required to achieve similarly high current densities were almost double that required in the NaOH–KOH–H_2O electrolyte (Table S8, ESI†). A major reason for this is the much higher ohmic resistance (R_{ohm}) of the aqueous electrolyte, not to mention the competitive HER that compromises the overall NH_3 FE as well.

Unravelling the Synergistic Enhancement for NO3RR in Fe_xCu_y@Ni Ternary System

A series of control experiments were conducted to understand the synergistic enhancement in catalytic activity and the crucial role of Fe in the Fe–Cu–Ni ternary system. The first of these instinctive controls is to examine the catalytic system without the introduction of the Fe component during the entire synthesis procedure, denoted as Fe_0Cu_8@Ni. To further test the impact of Ni presence, an electrode containing only Cu as the metal precursor (Cu_{10}) in the electrolyte bath was prepared. Additionally, the comparison between Cu_{10} and Cu foil also helps inspect the effect of extended surface area for Cu. The ternary Fe_4Cu_4@Ni (chemically, $Fe_4Cu_4Ni_4$) significantly outperforms the binary Cu–Ni (named Cu_8Fe_0, or chemically, Cu_4Ni_4) and the singular Cu (Cu_{10}) (Figure S8, ESI†).

The impact of Fe atoms on the synergistic enhancement of NO3RR performance can clearly be seen in the comparative NO3RR study on a series of electrodes with varying Fe : Cu ratios (from 0 : 8 to 7 : 1) under identical test conditions: at 3,000 mA/cm^2 at 100 °C in the NaOH–KOH–H_2O with 40 wt % of H_2O (Figure 3a). The

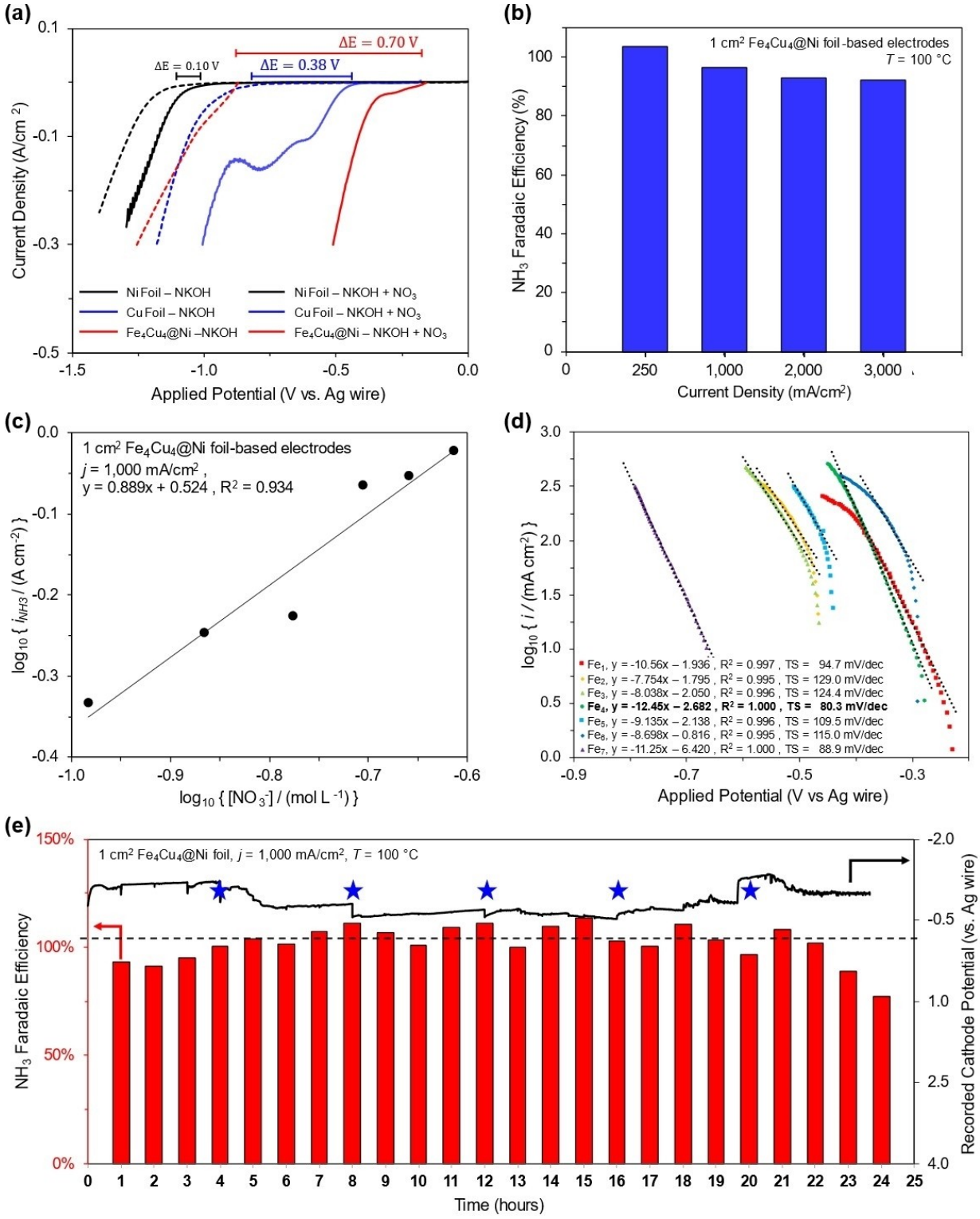

Figure 2. NO3RR performance of Fe_xCu_y@Ni catalytic system. **(a)** Voltammetric curves for NO3RR with different metals/catalysts as working electrodes with and without NO_3^- source in NaOH–KOH–H_2O (40 wt% water content). Test conditions: 50 mV/s of scan rate, 0.2 M of NO_3^- concentration, and 100 °C of cell temperature. **(b)** Coulombic efficiency of the Fe_4Cu_4@Ni catalyst at four typical current densities (0.2 M NO_3^- and 100 °C). **(c)** Electrochemical reaction-order plot on the Fe_4Cu_4@Ni catalyst operated at 1,000 mA/cm^2. **(d)** Tafel plot for Fe_xCu_y@Ni catalysts with different Fe : Cu ratios. **(e)** 24-hour stability test for NO3RR on the Fe_4Cu_4@Ni catalyst (1,000 mA/cm^2 and 100 °C), blue stars indicate times when the electrolyte was replenished with NO_3^-.

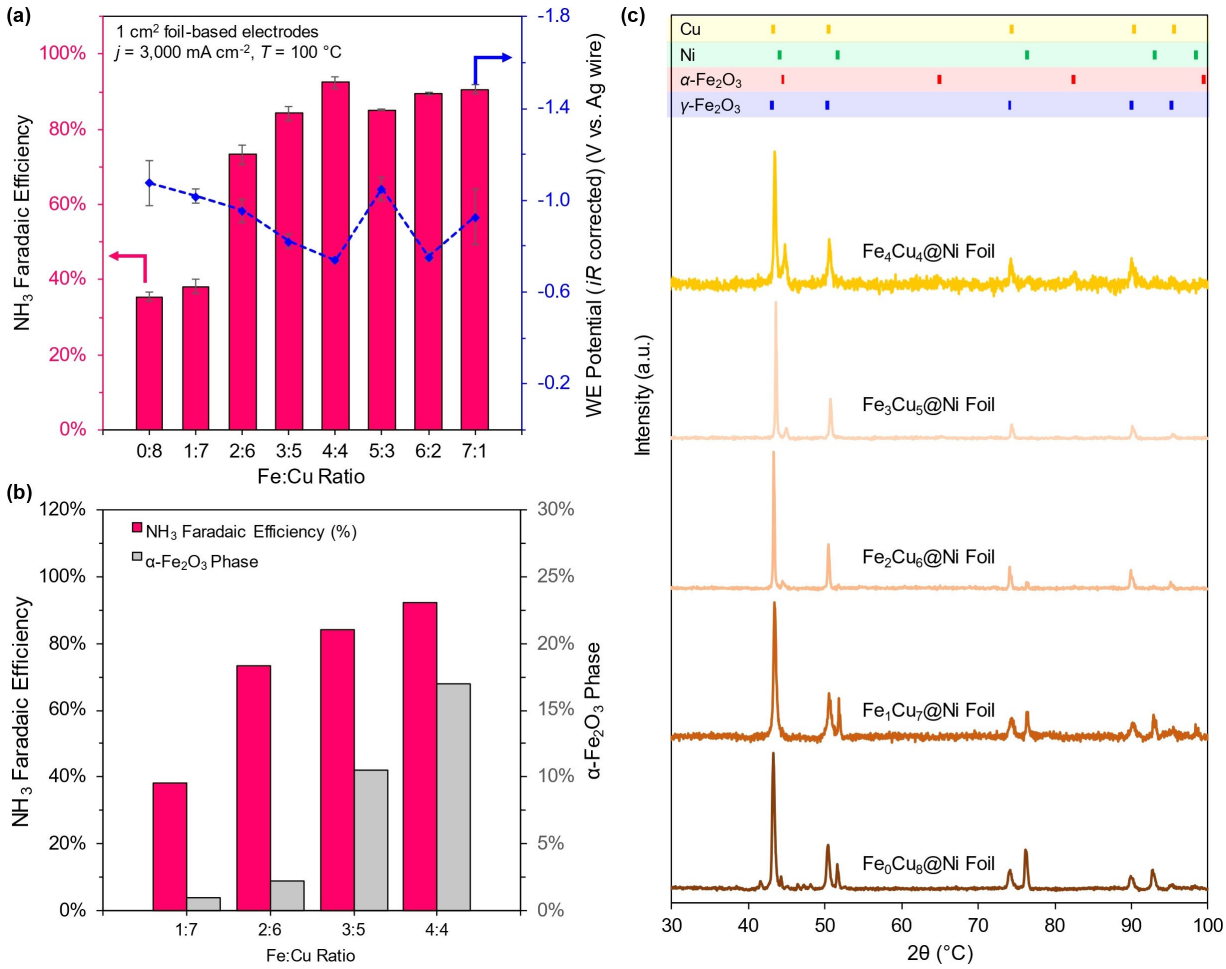

Figure 3. Coulombic efficiency and rationale of Fe_xCu_y@Ni catalytic system. (a) The impact of Fe:Cu ratio on the coulombic efficiency of Fe_xCu_y@Ni (3,000 mA/cm^2 and 100 °C) (b) The correlation between coulombic efficiency and the content of α-Fe_2O_3 phase in Fe_xCu_y@Ni, and (c) α-Fe_2O_3 phase evolution with increasing Fe content for selected Fe:Cu ratios.

NH_3 FE quickly increases with increasing Fe:Cu ratio until equimolar ratio (Fe_4Cu_4), beyond which it slightly slides down and plateaus. The observed cathode potential follows a fairly consistent trend: it shifts to less negative potential when raising the Fe:Cu ratio until reaching equimolar, and it goes slightly more negative afterward, albeit with a large fluctuation admittedly. Specifically, Fe_4Cu_4@Ni with the equimolar ratio showed the peak NH_3 FE 92.5 % as well as the least negative cathode potential of −0.75 V vs. Ag wire (iR corrected). Tafel slope analysis for the different Fe:Cu ratios also shows a trend similar to that observed for the ammonia FE and cathode potential: the Fe_4Cu_4@Ni exhibiting the lowest Tafel slope of just 80 mV dec^{-1} (Figure 2d).

To further understand the outstanding performance, we explored the electronic and atomic structure of the Fe–Cu–Ni catalyst in more detail through a high-resolution XPS analysis.

The XPS results for Fe_0Cu_8@Ni, Fe_1Cu_7@Ni, and Fe_4Cu_4@Ni revealed a significant change in the Cu *2p* and O *1s* profiles, while Ni *2p* profiles remained almost unfazed (see Figure 1i–k and Figure S6, ESI†). The Fe *2p* profile showed a marginal increase in intensity for Fe_4Cu_4@Ni and dominance of peaks attributed to the O_2/Fe/Cu $2p_{3/2}$ environment whereas for Fe_1Cu_7@Ni the peak with a binding energy of 723.5 eV was attributed to Fe_3O_4, i.e., a combination of Fe(III) and Fe(II) (Figure 1k and Figure S26, ESI†). For the O *1s* profile, we observed an increase in the overall intensity of the signal upon a small loading of Fe (i.e., Fe_1Cu_7@Ni) compared to the sample with no Fe, however, upon further increase to the equimolar ratios we observed a relative decrease in overall intensity in the O *1s* profile. For the Fe_0Cu_8@Ni O *1s* profile, the peaks between 529.0–532.0 eV, are attributed to oxygen atoms bound to the Cu and Ni, and hydroxyl groups[31,37] (Figure 1j). The same observation holds for samples Fe_1Cu_7@Ni and Fe_4Cu_4@Ni, however, we observe a significant plateauing and drop in intensity for Fe_4Cu_4@Ni between the 530.0–532.0 eV range (Figure 1j). These results suggest that the increased Fe loading results in the formation of an oxidation-resistant environment, especially for Cu, as observed in the Cu *2p* profile (Figure 1i). The Cu *2p* profile for both Fe_0Cu_8@Ni and Fe_1Cu_7@Ni contains peaks at 934.6, 941.9, and 943.0/944.8 eV (Fe_0Cu_8@Ni/Fe_1Cu_7@Ni) which are attributed to CuO $2p_{3/2}$, and CuO $2p_{3/2,sat}$. However, for

Fe_4Cu_4@Ni these aforementioned peaks are suppressed while the peaks for Cu $2p_{1/2}$ (952.5 eV) and Cu $2p_{3/2}$ (932.2 and 932.5 eV) become more intense. Moreover, the emergence of a peak at 933.8 eV attributed to the $CuFe_2O_4$ $2p_{3/2}$ and the absence of the CuO $2p_{3/2,sat}$ again suggests that the addition of Fe helps regulate the oxidation state of Cu species, primarily in the reduced metallic state. As also reported previously,[8] Cu-based binary alloys with high performance commonly rely on the Cu in its reduced state, (i.e., Cu^0) supporting the secondary metal to boost the overall performance.

Moreover, as previously established, the co-deposition of different metals does not guarantee the formation of a homogeneous solid solution. In fact, the deposit is more often a combination of different metallic phases.[38,39] As expected, probing the as-prepared Fe_4Cu_4@Ni electrode through XRD characterization revealed the existence of four distinct phases: pure Cu, pure Ni, Austenite (γ-Fe_2O_3), and Ferrite (α-Fe_2O_3) in Fe_xCu_y@Ni ternary system with varying intensities subject to the Fe : Cu ratio (Figure 3c and Table S9, ESI†). The intensity of α-Fe_2O_3 increases with increasing Fe content (Figure 3c), which is correlated well with an increase in the overall performance for NO3RR. Such correlation suggests that α-Fe_2O_3 may be the most active phase for NO3RR, among other catalytic phases and sites. Thus, the XPS and XRD results strongly suggest that the presence of Fe in the form of α-Fe_2O_3 suppresses the oxidation of Cu, thereby promoting a synergistic boost in overall eNO3RR performance in an ultrahigh alkalinity environment.

In addition, electrochemical impedance spectroscopic (EIS) analysis was conducted to examine the resistance of the Fe_xCu_y@Ni-based electrodes at different current densities. For these EIS experiments, a high concentration of NO_3^- was used to ensure that the change in electrolyte concentration was negligible and the electrolyte conductivity remained unchanged for each test. The same electrolyte was used for each electrode test. Consistently, EIS analysis revealed that the resistance of the cathode followed the same trend as that for the cathode potential and NH_3 FE for the NO3RR in our system: Fe_4Cu_4@Ni has the lowest cathode resistance of 0.240 Ωcm^2, compared with that of other Fe : Cu ratios (0.243–0.327 Ωcm^2) (Figure S24–25, Table S3, ESI†).

The highest NH_3 FE, the least negative cathode potential, the lowest Tafel slope, and the smallest electrode resistance clearly justify that the equimolar ratio is the optimum for Fe_xCu_y@Ni ternary catalyst for NO3RR at very high current densities.

The unique synergy between the Fe–Cu–Ni ternary system was thus demonstrated through the series of investigations reported above. However, intrigued by this unique performance, we are left with the lingering question: is this synergy unique to Fe–Cu–Ni in this ultrahigh alkalinity system, or whether elements other than Fe also have the potential to demonstrate such synergy? To explore this aspect, we shortlisted two additional candidates: Ruthenium (Ru) and Cobalt (Co), two elements that have exhibited extraordinary performance for eNO3RR in aqueous electrolytes[8,10,19,21,40] (performance summary available in Table S12, ESI†). Deploying the same strategy as that for the Fe–Cu–Ni ternary catalyst, we prepared the Ru–Cu–Ni and Co–Cu–Ni ternary catalysts with equimolar Ru : Cu : Ni and Co : Cu : Ni ratios. Under similar testing conditions as that of the Fe–Cu–Ni ternary electrode, we observed that at 1000 mA/cm^2 all three elements exhibit almost similar performance, i.e., NH_3 FE of 96 %, 94 %, 92 % for Fe, Ru, and Co respectively. However, as we ramp up the current densities to 2000 and 3000 mA/cm^2 the NH_3 FE drops dramatically for both Ru and Co, but the drop is sharper for Co. The same trend follows for ammonia production rates as well. Moreover, the overpotential required for both, Ru and Co for 1000, 2000, and 3000 mA/cm^2 current densities were also more negative than that needed for Fe-based ternary catalyst (see Table S10, ESI†). Therefore, we conclude that the high performance of the Fe–Cu–Ni ternary catalyst is due to the unique synergy between the Fe–Cu–Ni system.

Techno-Economic Analysis (TEA)

To examine the economic impact of introducing the Fe_4Cu_4@Ni catalyst in the ultrahigh alkalinity systems on the nitrate-to-ammonia process, we extended the techno-economic analysis (TEA) model established in our previous work[22] by including the additional costs associated with catalyst synthesis. As defined widely in TEA studies and adopted in this study, LTC = LCC + OPEX, where the LTC stands for the "Levelized total cost", and the LCC does for the "levelized capital cost".

The LCC is derived from normalizing the capital cost (CAPEX) with all produced products during the entire serving time, and also by considering the maintenance cost and financial cost over those service years. A major deviation in CAPEX lies in the catalyst synthesis: the customized Fe_4Cu_4@Ni in this work vs. a commercial Ni foam in our previous work, while keeping the same electrode area (3.36 m^2) and the same reactor volume (100 L). Based on the typical chronopotentiometric electrodeposition for making the Fe_4Cu_4@Ni (250 mA/cm^2, 75 % of current efficiency, 50 μm of resulting catalyst thickness), the amounts of chemicals and associated materials costs for the needed electrodepositing electrolyte were calculated. The cost of the Ni substrate and electricity for the electrodeposition process was also included. The CAPEX of the cathode was found to be $239 per 100 L-reactor, resulting in the total CAPEX for the entire electrolyzer to be $3,492 per system (a $371 increase from the system modeled for the commercial Ni foam). Additionally, the ultrahigh alkalinity environment and elevated temperature make the NH_3 separation intrinsic in the MFAEL, thus bypassing the need for additional purification units and thus restraining capital cost.

Thanks to the very low cost and high durability of earth-abundant materials for Fe_4Cu_4@Ni catalysts and electrodes, the contribution of the LCC is essentially insignificant,

thereby rendering the OPEX to denominate the LCC in the range of current densities (250–3000 mA/cm^2).

OPEX was obtained by accounting for the energy consumed for electrolysis (dependent upon the cell voltage, operating current density, and FE of NO3RR), electrolyte mixing, and cell heating. The industrial electricity price, 0.07 US$ per kWh, was used as the default energy cost for calculations. Driven largely by the significantly reduced cell voltage (1.68 V vs. 2.70 V), the adoption of Fe_4Cu_4@Ni catalyst (replacing the plain Ni wire mesh) lowered the OPEX by 38 % ($29.59 vs. $47.45 per kmol-$NH_3$) at the same current density of 250 mA/cm^2 (Table S4, ESI†). The LTC with Fe_4Cu_4@Ni catalyst is 63 % less than that with the commercial Ni foam ($30.68 vs. $48.53 per kmol-$NH_3$). Evidently, the significantly reduced cell voltage translates into the much-improved economic viability for the nitrate-to-ammonia electrochemical process.

In practice, a much larger current density is desirable. Taking the wastewater with a typical nitrate content of 100 ppm (NO_3^-–N) as an example, 250 mA/cm^2 of current density could only process 5.8 ton-wastewater/hour from the 100-L reactor system with 3.36 m^2 of total electrode area; but 1,000 mA/cm^2 and 3,000 mA/cm^2 may handle 23.2 and 69.5 ton-wastewater/hour, respectively, assuming 95 % of coulombic efficiency and 90 % of nitrate removal.

Of particular interest are the high-throughput applications, the LTC was examined at those larger current densities. As expected, the LTC increases substantially with rising current density, largely because of increasing cell voltage, given that coulombic efficiency is dropping slightly, Figure 4a. Compared with $30.68/kmol-$NH_3$ at 250 mA/cm^2, the LTC obtained was $42.34, $53.91, and $67.17 per kmol-$NH_3$, at 1,000, 2,000, and 3,000 mA/cm^2 of current density, respectively. It should be noted that the LTC with 3,000 mA/cm^2 of current density is still around the market cost of wastewater treatment ($65 per kmol-N[22]). The Fe_4Cu_4@Ni-enabled system allows for ultrahigh economic operation at a low rating of current density (such as 250 mA/cm^2) but also offers ultrahigh throughput operation (up to 3,000 mA/cm^2) without losing economic viability, and that too while ignoring the cost-benefit of ammonia as a value-added product.

The industrial price (0.07 US$/kWh) of electricity cost was used for all TEA results above, but we also recognize that cheaper electricity (0.03 US$/kWh) could be available when excessive renewable energy was harvested from wind and/or solar. Taking advantage of cheaper electricity is beneficial to achieve higher throughput operation, subject to a given cost constraint. The interplay between the electricity cost and applied cell voltage examined in this study is presented in a contour map, Figure 4b. Subject to any given applied cell voltage, the experimentally observed current density as well as the detected coulombic efficiency was incorporated in the TEA model for energy consumption, which led to the LTC by combining a given electricity cost (from 0 to 0.12 US$/kWh). In Figure 4b, one can clearly pair the operational cell voltage and the available electricity price to satisfy a given cost constraint (from 0–10 US$/kmol-$NH_3$ in black to >110 US$/kmol-$NH_3$ in red).

Conclusion

Advancing the field of NO3RR-to-NH_3 towards commercialization, we present herein an inexpensive, earth-abundant-metal-based ternary catalyst that enables low-cost and high-productivity NH_3 electrosynthesis from nitrates in an ultra-high alkalinity NaOH–KOH–H_2O electrolyte. The equimolar combination of Fe–Cu–Ni ternary catalyst enabled us to

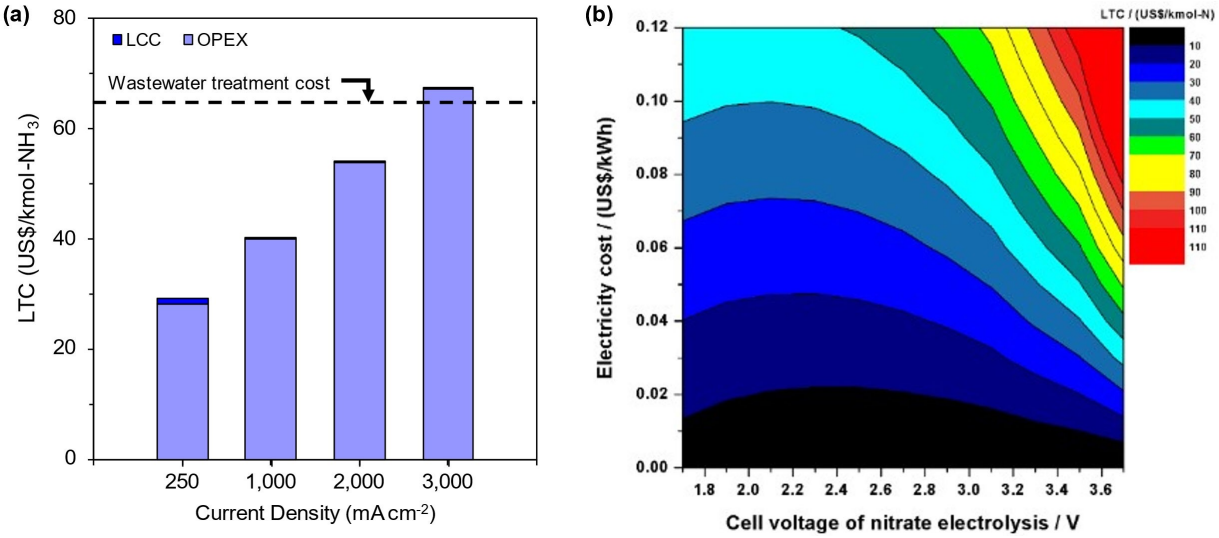

Figure 4. TEA results of NO3RR with Fe_4Cu_4@Ni electrode. (a) LTC at four typical current densities (0.07 US$/kWh). (b) Contour plot of LTC subject to the given electricity cost and the applied cell voltages. The TEA conducted in this study is based on a 100 L reactor and 3.36 m^2 of total electrode area with the ternary Fe_4Cu_4@Ni electrode (100 °C of cell temperature) and the ternary NaOH–KOH–H_2O electrolyte (40 wt % of water content).

achieve an unprecedented FE of 92.5 % at current density as high as 3,000 mA/cm^2 and a cell voltage of 3.83 V, while operation at milder current densities, e.g., 1,000 mA/cm^2, was realized at FE of 96.5 % and a cell voltage of only 2.40 V. In comparison with a plain Ni wire mesh cathode (our earlier work), the Fe–Cu–Ni system helps reduce the overall cell voltage by 30 % and the levelized cost of ammonia electrosynthesis by ~40 %.

As demonstrated in our earlier work, such a system can be integrated into existing wastewater treatment processes to upcycle waste nitrates into a value-added commodity like ammonia (or its' derivatives). A detailed technoeconomic analysis revealed that catalyst enhanced system can further reduce the current cost of N-removal (~65$ per kmol-N) to as low as $42.34 per kmol-N while operating at a current density of 1,000 mA/cm^2, and that too not accounting for the cost-benefit of the value-added ammonia as a product. Even integrating a pretreatment step for nitrate concentration by a low-energy cost-effective electrodialysis process (costing $5.75 per kmol-$NO_3^-$)[22] does not blemish its commercialization prospects, and the combined system maintains its competitive edge over existing technologies. Furthermore, such a system can potentially increase the handling capacity of existing wastewater treatment plants by expediting the handling time by an order of magnitude.

This discovery presents a commercially viable pathway for ammonia electrosynthesis from nitrates, helping reduce the dependence upon the energy-intensive Haber–Bosch process while tackling the global sustainability challenge. At the same time, it presents an incentive to explore a sustainable route for direct fixation of N_2 into NO_x and eventually drive a shift away from the heavy reliance on the current Haber–Bosch process.

Author Contributions

The research article was planned, designed, and executed by **U.B. Shahid** and played a central role in the conceptualization of the study, data collection, analysis, and interpretation of the results. Additionally, **U.B. Shahid** wrote the first draft of the manuscript which was subsequently revised based on the valuable feedback from **S. Gu** and **M. Shao**. **Y. Kwon** provided valuable support by assisting with the preparation of electrocatalysts and determining the nitrate concentration of samples. **Y. Yuan** also supported the research by running several control tests for NO3RR, helping determine nitrate and NH_3 concentrations, and helping prepare Figures. Their diligent work and attention to detail ensured accurate and reliable data for the study. **S. Gu** made substantial contributions during the review process, providing valuable insights and feedback that enhanced the quality of the manuscript. Additionally, **S. Gu** contributed to the technoeconomic analysis section, bringing their expertise to bear on the economic aspects of the research. **M. Shao** supervised the entire research project, providing guidance and oversight throughout the process. His extensive knowledge and experience in the field were instrumental in shaping the study and ensuring its successful completion. All authors reviewed and approved the final version of the manuscript, acknowledging their respective contributions to the research.

Acknowledgements

The authors acknowledge the support from the Research Grant Council (16304821, 16310419, and 16308420), Innovation and Technology Commission (grant no. ITC-CNER-C14EG03) of the Hong Kong Special Administrative Region. S. Gu acknowledges the financial support by the U.S. National Science Foundation through the following programs: Future Manufacturing (# 2036944), ECO-CBET (# 2219172), and EPSCoR (# 2316482). U.B. Shahid acknowledges his Hong Kong PhD Fellowship granted by the Research Grant Council.

Conflict of Interest

The authors declare no competing interests.

Data Availability Statement

The data that support the findings of this study are available from the corresponding author upon reasonable request.

[1] S. Fields, *Environ. Health Perspect.* **2004**, *112*, A557–A563.
[2] N. Lehnert, H. T. Dong, J. B. Harland, A. P. Hunt, C. J. White, *Nat. Chem. Rev.* **2018**, *2*, 278–289.
[3] P. Heffer, M. Prud'homme, *Int. Nitrogen Initiat. Conf.* **2016**, 1–11.
[4] M. Ward, R. Jones, J. Brender, T. de Kok, P. Weyer, B. Nolan, C. Villanueva, S. van Breda, *Int. J. Environ. Res. Public Health* **2018**, *15*, 1557.
[5] Q. Gao, H. S. Pillai, Y. Huang, S. Liu, Q. Mu, X. Han, Z. Yan, H. Zhou, Q. He, H. Xin, H. Zhu, *Nat. Commun.* **2022**, *13*, 2338.
[6] W. He, J. Zhang, S. Dieckhöfer, S. Varhade, A. C. Brix, A. Lielpetere, S. Seisel, J. R. C. Junqueira, W. Schuhmann, *Nat. Commun.* **2022**, *13*, 1129.
[7] Z.-Y. Wu, M. Karamad, X. Yong, Q. Huang, D. A. Cullen, P. Zhu, C. Xia, Q. Xiao, M. Shakouri, F.-Y. Chen, J. Y. Kim, Y. Xia, K. Heck, Y. Hu, M. S. Wong, Q. Li, I. Gates, S. Siahrostami, H. Wang, *Nat. Commun.* **2021**, *12*, 2870.
[8] F.-Y. Chen, Z.-Y. Wu, S. Gupta, D. J. Rivera, S. V. Lambeets, S. Pecaut, J. Y. T. Kim, P. Zhu, Y. Z. Finfrock, D. M. Meira, G. King, G. Gao, W. Xu, D. A. Cullen, H. Zhou, Y. Han, D. E. Perea, C. L. Muhich, H. Wang, *Nat. Nanotechnol.* **2022**, *17*, 759–767.
[9] Y. Wang, A. Xu, Z. Wang, L. Huang, J. Li, F. Li, J. Wicks, M. Luo, D.-H. Nam, C.-S. Tan, Y. Ding, J. Wu, Y. Lum, C.-T. Dinh, D. Sinton, G. Zheng, E. H. Sargent, *J. Am. Chem. Soc.* **2020**, *142*, 5702–5708.
[10] J. Li, G. Zhan, J. Yang, F. Quan, C. Mao, Y. Liu, B. Wang, F. Lei, L. Li, A. W. M. Chan, L. Xu, Y. Shi, Y. Du, W. Hao, P. K. Wong, J. Wang, S.-X. Dou, L. Zhang, J. C. Yu, *J. Am. Chem. Soc.* **2020**, *142*, 7036–7046.

[11] X. Zhao, G. Hu, F. Tan, S. Zhang, X. Wang, X. Hu, A. V. Kuklin, G. V. Baryshnikov, H. Ågren, X. Zhou, H. Zhang, *J. Mater. Chem. A* **2021**, *9*, 23675–23686.
[12] Q. Hu, Y. Qin, X. Wang, Z. Wang, X. Huang, H. Zheng, K. Gao, H. Yang, P. Zhang, M. Shao, C. He, *Energy Environ. Sci.* **2021**, *14*, 4989–4997.
[13] S. Ye, Z. Chen, G. Zhang, W. Chen, C. Peng, X. Yang, L. Zheng, Y. Li, X. Ren, H. Cao, D. Xue, J. Qiu, Q. Zhang, J. Liu, *Energy Environ. Sci.* **2022**, *15*, 760–770.
[14] R. Daiyan, T. Tran-Phu, P. Kumar, K. Iputera, Z. Tong, J. Leverett, M. H. A. Khan, A. Asghar Esmailpour, A. Jalili, M. Lim, A. Tricoli, R.-S. Liu, X. Lu, E. Lovell, R. Amal, *Energy Environ. Sci.* **2021**, *14*, 3588–3598.
[15] F. Du, J. Li, C. Wang, J. Yao, Z. Tan, Z. Yao, C. Li, C. Guo, *Chem. Eng. J.* **2022**, *434*, 134641.
[16] Z. Fang, Z. Jin, S. Tang, P. Li, P. Wu, G. Yu, *ACS Nano* **2022**, *16*, 1072–1081.
[17] N. Zhang, J. Shang, X. Deng, L. Cai, R. Long, Y. Xiong, Y. Chai, *ACS Nano* **2022**, *16*, 4795–4804.
[18] X. Fan, L. Xie, J. Liang, Y. Ren, L. Zhang, L. Yue, T. Li, Y. Luo, N. Li, B. Tang, Y. Liu, S. Gao, A. A. Alshehri, Q. Liu, Q. Kong, X. Sun, *Nano Res.* **2022**, *15*, 3050–3055.
[19] Z. Li, J. Liang, Q. Liu, L. Xie, L. Zhang, Y. Ren, L. Yue, N. Li, B. Tang, A. A. Alshehri, M. S. Hamdy, Y. Luo, Q. Kong, X. Sun, *Mater. Today Phys.* **2022**, *23*, 100619.
[20] H. Liu, X. Lang, C. Zhu, J. Timoshenko, M. Rüscher, L. Bai, N. Guijarro, H. Yin, Y. Peng, J. Li, Z. Liu, W. Wang, B. R. Cuenya, J. Luo, *Angew. Chem.* **2022**, *134*, DOI 10.1002/ange.202202556.
[21] X. Deng, Y. Yang, L. Wang, X. Fu, J. Luo, *Adv. Sci.* **2021**, *8*, DOI 10.1002/advs.202004523.
[22] Y. Chen, P. Ammari-Azar, H. Liu, J. Lee, Y. Xi, M. J. Castellano, S. Gu, W. Li, *EES Catal.* **2023**, *1*, 504–515.
[23] M. Xu, Q. Xie, D. Duan, Y. Zhang, Y. Zhou, H. Zhou, X. Li, Y. Wang, P. Gao, W. Ye, *ChemSusChem* **2022**, *15*, DOI 10.1002/cssc.202200231.
[24] Y. Xu, Z. Peng, Y. Han, H. Zhong, J. Yang, Y. Cao, *ChemSusChem* **2022**, *15*, DOI 10.1002/cssc.202102450.
[25] Q. Liu, L. Xie, J. Liang, Y. Ren, Y. Wang, L. Zhang, L. Yue, T. Li, Y. Luo, N. Li, B. Tang, Y. Liu, S. Gao, A. A. Alshehri, I. Shakir, P. O. Agboola, Q. Kong, Q. Wang, D. Ma, X. Sun, *Small* **2022**, *18*, DOI 10.1002/smll.202106961.
[26] J. Yuan, Z. Xing, Y. Tang, C. Liu, *ACS Appl. Mater. Interfaces* **2021**, *13*, 52469–52478.
[27] Y. Wang, L. Zhang, Y. Niu, D. Fang, J. Wang, Q. Su, C. Wang, *Green Chem.* **2021**, *23*, 7594–7608.
[28] N. Guillet, P. Millet, in *Hydrog. Prod.*, Weinheim, Germany **2015**, pp. 117–166.
[29] H. Li, D. H. Robertson, J. Q. Chambers, D. T. Hobbs, *J. Electrochem. Soc.* **1988**, *135*, 1154–1158.
[30] B. P. Dash, S. Chaudhari, *Water Res.* **2005**, *39*, 4065–4072.
[31] P. Zhang, L. Li, D. Nordlund, H. Chen, L. Fan, B. Zhang, X. Sheng, Q. Daniel, L. Sun, *Nat. Commun.* **2018**, *9*, 381.
[32] M. Gong, H. Dai, *Nano Res.* **2015**, *8*, 23–39.
[33] K. H. Kim, J. Y. Zheng, W. Shin, Y. S. Kang, *RSC Adv.* **2012**, *2*, 4759.
[34] A. M. E. Khalil, O. Eljamal, S. Jribi, N. Matsunaga, *Chem. Eng. J.* **2016**, *287*, 367–380.
[35] S. Kerkeni, E. Lamy-Pitara, J. Barbier, *Catal. Today* **2002**, *75*, 35–42.
[36] D.-W. Cho, H. Song, F. W. Schwartz, B. Kim, B.-H. Jeon, *Chemosphere* **2015**, *125*, 41–49.
[37] L. Zhuang, L. Ge, Y. Yang, M. Li, Y. Jia, X. Yao, Z. Zhu, *Adv. Mater.* **2017**, *29*, DOI 10.1002/adma.201606793.
[38] S. Vesztergom, A. Dutta, M. Rahaman, K. Kiran, I. Zelocualtecatl Montiel, P. Broekmann, *ChemCatChem* **2021**, *13*, 1039–1058.
[39] I. Najdovski, P. Selvakannan, A. P. O'Mullane, *RSC Adv.* **2014**, *4*, 7207.
[40] J. Wang, C. Cai, Y. Wang, X. Yang, D. Wu, Y. Zhu, M. Li, M. Gu, M. Shao, *ACS Catal.* **2021**, *11*, 15135–15140.

Manuscript received: February 21, 2024
Accepted manuscript online: March 22, 2024
Version of record online: April 17, 2024